

A case study of a monsoon low that formed over the sea and intensified over land as seen in the ECMWF analyses

Gerard Kilroy^{a*}, Roger K. Smith^a, Michael T. Montgomery^b, Billy Lynch^c and Craig Earl-Spurr^c

^a *Meteorological Institute, Ludwig-Maximilians University of Munich, Munich, Germany*

^b *Dept. of Meteorology, Naval Postgraduate School, Monterey, CA*

^c *Bureau of Meteorology, Darwin, Australia*

*Correspondence to: Dr. Gerard Kilroy, Meteorological Institute, Ludwig-Maximilians University of Munich, Theresienstr. 37, 80333 Munich, Germany. E-mail: gerard.kilroy@lmu.de

A case study is presented of a tropical low that formed near Darwin, Australia, during the monsoon and subsequently intensified over land. The study is based on European Centre for Medium Range Weather Forecast (ECMWF) analyses. Interpretations of the formation over the sea are given in terms of vorticity dynamics. The thermodynamic support for the intensification and maintenance of the low over land is investigated also. The analyses indicate that the intensification of the low depends on repeated bursts of deep convection occurring near the centre of the circulation that promote the further concentration of vorticity near the centre. This concentration of vorticity increases the local circulation about the centre, which amounts to increasing the local tangential wind speed and, through approximate gradient wind balance above the boundary layer, to a lowering of the central pressure. It is found that the horizontal transport of moisture into a mesoscale column centred on the low is approximately equal to the moisture lost by precipitation so that total precipitable water levels are not rapidly depleted over land. While the contribution to the overall moisture budget by surface fluxes is comparatively small, these fluxes are necessary to maintain conditionally unstable conditions near the vortex centre so that deep convective bursts can continue to occur there, even when the system is located far inland.

Copyright © 2016 Royal Meteorological Society

Key Words: Tropical depressions; tropical lows, tropical cyclogenesis, monsoon

Received March 1, 2016; Revised ; Accepted

Citation: . . .

1. Introduction

During the Australian ‘Wet Season’ (November–April) a trough of low pressure lies south of the equator with the trough axis coinciding approximately with the “monsoon shear line”. The latter separates westerly flow to the north from easterly flow to the south (McBride and Keenan 1982). Early in the wet season, the trough and shear line lie over the seas to the north of Australia, but later they may move southwards. The latitude of the trough axis may vary considerably with longitude at any one time and parts may

lie over the continent. It is typical for low pressure systems to develop at spatial intervals along the trough. Since water temperatures to the north of Australia can be as high as 30°C, lows that form over the ocean frequently develop into tropical cyclones. However, sometimes lows may form and intensify while remaining over land and like tropical cyclones, these systems pose a challenge to forecasters in the region. A pioneering and insightful analysis of tropical cyclogenesis in the Australian region is provided by McBride and Keenan (1982).

While much is now known about the structure of tropical cyclones and the mechanisms by which they intensify (e.g. Montgomery and Smith 2014, Smith and Montgomery 2015), rather less is known about the structure of intensifying tropical lows over land as well as the role of deep convection in their maintenance. Even though the lows form over a region with relatively sparse conventional data coverage, current numerical forecast models such as that of the European Centre for Medium range Weather Forecasts (ECMWF) sometimes show considerable skill in predicting both their formation and evolution. For this reason it is instructive to analyze such forecasts, or better still the analyses that are based in part on the previous forecast and in part on available observations.

As a step in this direction, Smith *et al.* (2015) examined three lows that formed in the Australian monsoon during Jan 2013 on the basis of ECMWF analyses. All three lows formed on the monsoon shear line and two of them became tropical cyclones. Interpretations of genesis were given in terms of vorticity dynamics and applied equally to one initial development over land as well as two over the sea. It was found that the intensification of a low requires repeated bursts of deep convection near the centre of the gyre to promote the further concentration of vorticity near the centre. This vorticity concentration increases the local circulation about the centre, which amounts to increasing the local tangential wind speed and, through approximate gradient wind balance above the boundary layer, to a lowering of the central pressure.

1.1. Two scientific questions

Two important scientific questions concerning the formation and intensification of tropical lows over land were raised by Smith *et al.* (2015). One question is whether their intensification is fundamentally different from that of tropical cyclones over the sea? Another question is whether the marsupial paradigm proposed by Dunkerton *et al.* (2009) is useful in understanding the formation of tropical cyclones in the monsoon regime of northern Australia, and indeed for monsoon depressions over land.

The marsupial paradigm refers to the nurturing role of a tropical wave in the formation of tropical depressions. The hybrid wave-vortex structure was likened to the development of a marsupial infant in its mothers pouch. By analogy, a juvenile proto-vortex is carried along by its parent wave until the proto-vortex is strengthened into a self-sustaining entity. For tropical storms developing within tropical waves, the recirculating flow in the wave's critical layer corresponds to the "pouch" where the wave and mean-flow speeds are similar. The centre of the pouch is defined as the intersection of the trough axis and the critical-latitude¹, which is oriented parallel to the easterly jet. Storm formation occurs near this so-called sweet spot.

Support for the relevance of the marsupial paradigm to tropical low formation in the monsoon regime was found in the three lows investigated by Smith *et al.* (2015). They showed that for these cases, low formation occurred only in regions where the Okubo-Weiss parameter was large and positive near the centre of the nascent vortex indicating a minimal detrimental effect of shearing deformation on

the vortex (Rozoff *et al.* 2006, Montgomery *et al.* 2012). However, a more complete answer to the latter question calls for an investigation of the supply of moisture to sustain deep convection, particularly in the case of lows that form and/or intensify over land.

1.2. Thermodynamic support for intensification over land

Kaplan and DeMaria (1995) found that when a tropical low moves inland and is cut off from the large heat fluxes from the underlying ocean, it rapidly decays with an exponential time constant of around 10 h. There are some exceptions to this behaviour with certain types of terrain being less detrimental to storm decay than others. Shen *et al.* (2002) found that large heat fluxes over swampy terrain leads to redevelopment over land, and this terrain provides also larger surface fluxes of moisture when compared to the arid desert terrain of Northern Australia.

Emanuel *et al.* (2008) sought to explain the redevelopment of warm-core cyclones over land in Northern Australia using an axisymmetric atmospheric model coupled to a simple model of the upper ocean. The basis of the model is presented by Emanuel (1995) and is designed around the assumption of slantwise convective neutrality along surfaces of constant absolute angular momentum. They found that warm-core cyclones can indeed intensify when the underlying soil is sufficiently warm and wet and the system is maintained by sensible heat and moisture (latent heat) transfer from the soil. In this model, landfall is simulated by setting the surface enthalpy flux coefficient to a value that diminishes with land elevation (Emanuel *et al.* 2004). They conclude that when the storms are sufficiently isolated from their oceanic source of moisture, the rainfall they produce is insufficient to keep the soil wet enough to transfer significant quantities of heat², and the storms then decay rapidly.

The strong focus on surface fluxes over land has no doubt been influenced by the WISHE paradigm for tropical cyclone intensification, which invokes a multi-step feedback process between surface enthalpy fluxes and a spin up of the tangential winds. This widely-accepted feedback mechanism has been shown to be non-essential in explaining the intensification of tropical cyclones (Montgomery *et al.* 2009, 2014).

Evans *et al.* (2011) performed numerical simulations of tropical cyclone Erin (2007), a storm that made landfall from the Gulf of Mexico and underwent re-intensification over the central United States. They found that the Emanuel *et al.* (2008) along-track tropical cyclone rainfall feedback mechanism to be "of minimal importance to the evolution of the vortex". They concluded that "the final intensity of the simulated (and presumably observed) vortex appears to be closely linked to the maintenance of boundary layer moisture over pre-existing near-climatological soil moisture content along the track of the vortex and well above climatological soil moisture content." They noted that "variations in soil moisture content result in impacts upon the boundary layer thermodynamic environment via boundary layer mixing. Greater soil moisture content results in weaker mixing, a shallower boundary layer, and greater moisture and instability. Differences in the intensity of

¹The critical latitude on a particular pressure surface is defined by the locus of points satisfying $U = c_{px}$, where c_{px} denotes the zonal phase speed of the wave and U denotes the local zonal wind.

²Emanuel *et al.* (2008) do not make a distinction between sensible and latent heat.

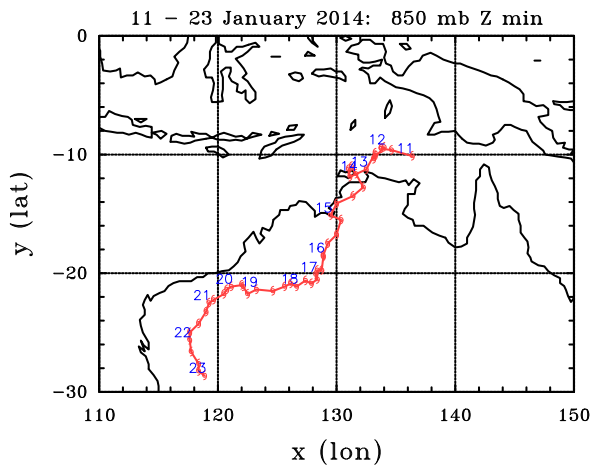


Figure 1. Track of the tropical low from 11–23 Jan 2014. Positions of the minimum geopotential at 850 mb indicated by cyclone symbols every 6 h. Positions at 00 UTC shown by date.

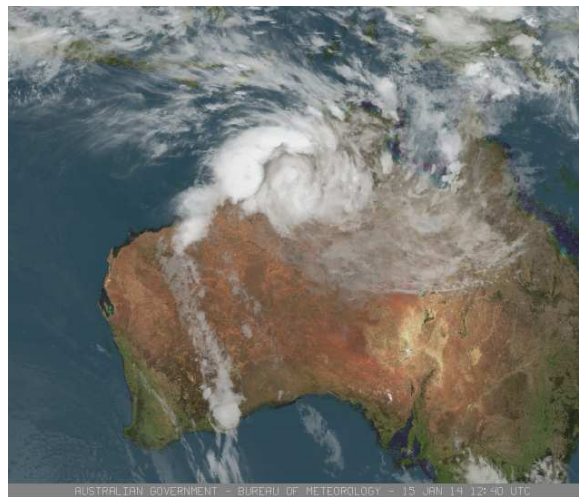


Figure 2. Visible satellite image on the 15 Jan 2014 at 12:40 UTC.

convection that develops and its accompanying latent heat release aloft result in greater warm-core development and surface vortex intensification within the simulations featuring greater soil moisture content.”

Sharkov *et al.* (2012) sought to determine the necessary amount total precipitable water (TPW) for genesis in the surrounding atmosphere over the ocean. They found that there is a critical value (60 kg m^{-2}) of TPW over a region surrounding the tropical cyclone so that it persists longer than 24 h. Interestingly, Emanuel *et al.* (2008) did not consider the horizontal transport of moisture into the vortex, a potentially large source of moisture that may help sustain the system, even though some degree of surface fluxes are indeed necessary for a vortex to be able to deepen (e.g. Malkus and Riehl 1960). For one thing, such moisture fluxes are required maintain conditional instability and thereby to sustain deep convection within the vortex circulation.

1.3. The present study

In this paper we examine a further case of the formation and structure of a tropical low in the Australian monsoon regime. As in Smith *et al.* (2015), the study is based largely on ECMWF analyses. Unlike in the cases studied by Smith *et al.* (2015), the low intensified as it moved southwards over the land. Here we study the life cycle of the disturbance prior to its extratropical transition. The objective is to provide a vorticity perspective of genesis and an analysis of the moisture supply necessary to support intensification.

The paper is organized as follows. First, in section 2 we present details of the data sets on which our analyses are based. A description of the evolution of the system from a forecasters perspective is given in the section 3. In section 4 we introduce the necessary diagnostic tools which we use to explain the formation and intensification of the low. In section 5 we examine the genesis of the low and its evolution after landfall. In section 6 we present the conclusions.

2. Data sets

The ECMWF analyses used for this study are available at the surface and at 25 pressure levels between 1000 mb and 1 mb. They cover the domain from 100°E to 160°E , from

the Equator to 30°S , and have a horizontal grid spacing of 0.125 deg . The case study is based largely on selected kinematic and thermodynamical fields extracted from these analyses, supplemented by geostationary satellite imagery from the Japanese Meteorological Satellite (MTSAT). The analyses, which are obtained from a global 4DVAR analysis and prediction system, are considered by forecasters to be as good as any available.

3. Low evolution from a forecaster’s perspective

During the early hours of 11 Jan 2014, convection within a deepening monsoon trough was strongest over the Arafura Sea to the north of the Northern Territory’s “Top End” and west of a previously identified weak circulation near Cape York Peninsula, south of New Guinea. This region of strong convection was identified also as the region of strongest local vertical vorticity. Scatterometry³ later in the day indicated that a new low had formed in this region. This new low is the focus of our study. The track of this low, as determined by the minimum geopotential at 850 mb, is shown in Fig. 1.

The environment was broadly favourable with a deep layer of moist air and a deep (up to 500 mb) and almost upright system (some overlap of the 850 mb and 500 mb centres). Deep vertical shear was moderate (about 10 m s^{-1} from the east), but not hugely detrimental. From 00 UTC⁴ on 11 Jan, pressure falls within the monsoon trough were of the order of 3 mb per day, although some locations were measuring 4–6 mb per day. The low remained poorly defined within the monsoon trough with a large uncertainty in its position until on 12 Jan when persistent convection began to develop. Up until this point, persistent convection near the low was almost non-existent. Overnight of 12 Jan and into 13 Jan, the low tracked west to north of Cobourg Peninsula, about 300 km northeast of Darwin, with central pressures falling below 1000 mb. Thunderstorms finally started flaring near the circulation centre during this time and at 06 UTC on 13 Jan a Dvorak initial classification (Current Intensity (CI)

³Scatterometry is a method for determining near surface wind speed and direction over oceans and consists of a satellite borne microwave radar sensor used to measure reflection or scattering effects produced by wind waves.

⁴Universal Time Coordinated. Note that local time is $\frac{1}{2}$ h ahead of UTC.

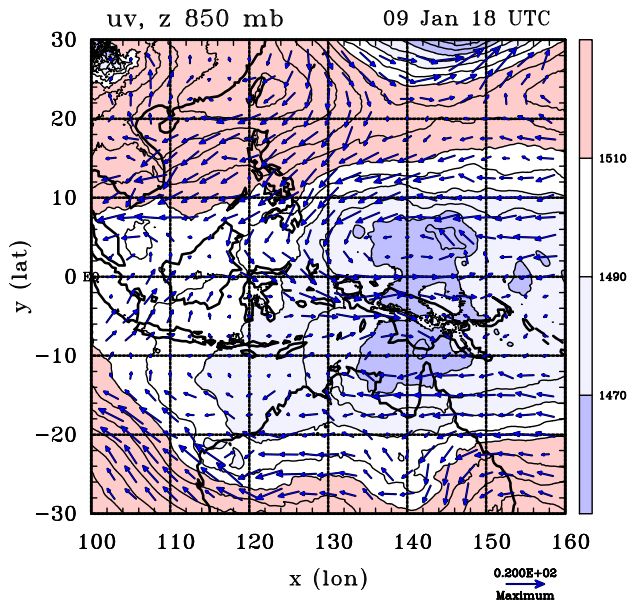


Figure 3. Isoleths of 850 mb geopotential height for an extended domain showing also the northern hemisphere on 9 Jan 2014 at 18 UTC. Shading indicates weak low pressure systems either side of the equator near 140°E. Contour interval for geopotential height 10 m, values for shaded regions given in label bar. Shown also are wind vectors at 850 mb.

1.0) was assigned by the Darwin Tropical Cyclone Warning Centre.

Model guidance had been mixed up to this point. The ACCESS suite (Australian Community Climate and Earth-System Simulator) was predicting the most intense storm, whereas other models including the ECMWF model were not indicating intensification. ECMWF was also indicating a monsoon low structure with the strongest winds away from the low centre. ECMWF ensemble probabilities for a tropical storm barely exceeded 20%. All models were indicating a south-westward movement towards the Kimberley region of Western Australia, but it was a fine line between a track that moved over the Timor Sea versus a track that moved over the western Top End south of Darwin. Over time the consensus track was shifting further east and eventually over land.

The Darwin Tropical Cyclone Warning Centre began issuing advice to the community on 13 Jan, with a Tropical Cyclone Watch issued at 01:30 UTC for the possibility of the low developing into a tropical cyclone in 24–48 h. However, overnight on 13 Jan the low took a southerly track and based on an analysis of surface observations, crossed the coast just after 00 UTC on 14 Jan, about 100 km east of Darwin, with a CI of 1.0. The mid-level centre, as tracked on radar, was now displaced west of the low level centre indicating the effects of easterly vertical shear.

Although the consensus track was over land, the uncertainty still allowed for movement into the Timor Sea and subsequent intensification. At 04:30 UTC on 14 Jan the Tropical Cyclone Watch was upgraded to a Tropical Cyclone Warning, for the possibility of a tropical cyclone forming in the southern Timor Sea within 24 h. However, as the low continued to track south-westward over land, the time available to move over water and intensify diminished and at 22:30 UTC on 14 Jan the Tropical Cyclone Warning was cancelled.

Heavy rain developed in the Darwin region following the passage of the low with reports of flash flooding. The

heaviest 24 h rainfall during this event was 205.6 mm recorded at Elizabeth Valley (40 km southeast of Darwin) in the 24 h period to 23:30 UTC on 14 Jan. Figure 2 shows a satellite image of the system on 15 Jan at 12:40 UTC. The widespread rainfall continued as the low tracked across the western Top End and moved south on 15 Jan. Despite being over land the system continued to deepen as it moved southward over the Tanami Desert and it was located favourably beneath the upper level ridge.

On 17 Jan the system had a central pressure of 992 mb and headed in a westerly direction across the interior of Western Australia and into the Pilbara region, passing southeast of Marble Bar on 20 Jan. The system reached its lowest central pressure of 989 mb on 21 Jan and then rapidly weakened as it recurved to the southeast before being captured in the mid-latitude westerly airstream. The low maintained remarkable structure while over land until it was captured by this westerly airstream.

4. Vorticity and Okuba-Weiss diagnostics

In this section we first introduce the necessary diagnostic tools which we use to explain the formation and intensification of the low. Smith *et al.* (2015) showed that insight into the monsoon and the low pressure systems that form within could be obtained by an analysis of the vorticity field and its time evolution. In pressure coordinates, the vorticity tendency equation has a particularly concise form in which the local tendency of absolute vorticity ζ_a can be written as the horizontal divergence of a horizontal flux (Haynes and McIntyre 1987, Raymond and López Carillo 2011, Tory *et al.* 2012, Raymond *et al.* 2014), i.e.

$$\frac{\partial \zeta_a}{\partial t} = -\nabla_h \cdot \mathbf{F}_{\zeta_a}, \quad (1)$$

where $\mathbf{F}_{\zeta_a} = \mathbf{F}_{af} + \mathbf{F}_{naf}$, $\mathbf{F}_{af} = \mathbf{u}_h \zeta_a$ and $\mathbf{F}_{naf} = -\zeta_h \omega + \mathbf{k} \wedge \mathbf{F}_{fri}$. Here \mathbf{u}_h is the horizontal velocity vector, ζ_h is the horizontal component of vorticity, ω is the material derivative of pressure and plays the role of “vertical velocity” in pressure coordinates, \mathbf{F}_{fri} is the horizontal force per unit mass due to molecular effects and sub-grid-scale eddy momentum fluxes, and \mathbf{k} is a unit vector in the vertical. More details about the benefits of analysing vertical vorticity in this form is given in Smith *et al.* (2015).

While useful in characterizing local rotation, vertical vorticity may be associated with regions of strong horizontal shear deformation, which is detrimental to the formation of concentrated vortices. Favourable regions for vortex formation are those where the vorticity is dominated by pure rotation. Dunkerton *et al.* (2009) used depictions of the Okuba-Weiss (OW) parameter (see appendix in Smith *et al.* 2015) to highlight regions within the broadscale flow that tend to be most immune to horizontal shear deformation, i.e. regions where the flow is rotationally dominant. These are regions where convectively generated patches of vertical vorticity are most capable of congealing to form a monopole structure. We examine such diagnostics here also.

5. Low development as seen in the ECMWF analyses

We divide our analysis of the low into two time periods: the early period of formation over the sea, where we examine the initial intensification of the low from a vorticity

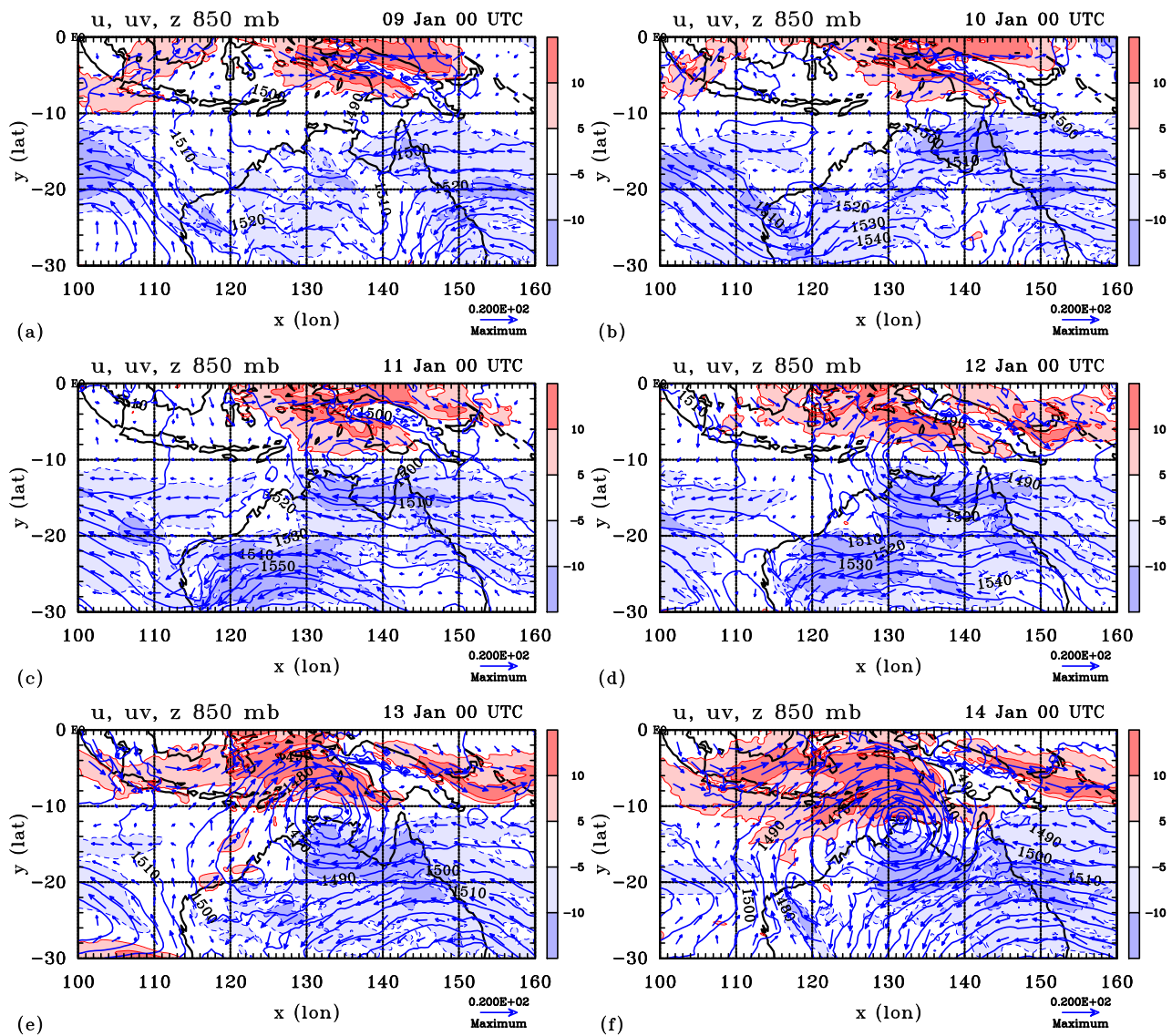


Figure 4. Wind vectors at 850 mb together with contours of the zonal wind component and geopotential height at 00 UTC on (a) 9 Jan, (b) 10 Jan, (c) 11 Jan, (d) 12 Jan, (e) 13 Jan and (f) 14 Jan, 2014 illustrating the formation and intensification of the low. Westerly wind component greater than 5 m s^{-1} shaded pink, that greater than 10 m s^{-1} shaded red. Easterly winds greater than 5 m s^{-1} in magnitude shaded light blue, those greater than 10 m s^{-1} in magnitude shaded blue. Contour interval for geopotential height 10 m (blue contours). Solid contours positive, dashed contours negative. Wind vectors should be compared to the reference vector (20 m s^{-1}) at the bottom right of each panel.

perspective, and the period of subsequent intensification over land, where we focus on the moisture supply needed to support the intensification process. We take landfall to be at 06 UTC 14 Jan, when in the ECMWF analyses (see Fig. 1) the minimum geopotential of the system crossed the coast.

5.1. Formation

Figure 3 shows geopotential heights at 850 mb at 18 UTC 9 Jan for a region north and south of the equator. A notable feature is a region of low geopotential straddling the equator with local minima in each hemisphere. This structure is characteristic of an equatorially-trapped $n = 1$ Rossby wave (ER wave). In animations of these fields (not shown), the two lows move polewards and westwards over 10 days, with the northern hemisphere low remaining weaker than the southern hemisphere one. Consistent also with an ER wave structure is a band of strong westerlies at the equator known as a westerly wind burst.

The southern hemisphere low of the ER wave appears to be the precursor disturbance leading to the low of interest here and presumably provided a favourable “pouch” in which the low was able to intensify. Tropical cyclogenesis within ER waves is described in detail by Molinari *et al.* (2007).

Figure 4 shows the wind structure at 850 mb together with wind vectors and contours of the zonal wind component and geopotential height at 00 UTC from 9 Jan to 14 Jan 2014. On 9 Jan there is a region of locally strong westerlies near Papua New Guinea and a weak cyclonic gyre south of Papua New Guinea within a larger area of low geopotential heights, but the easterly winds to the south of the island in the belt from 130°E to 160°E are relatively light. In the days that follow, the easterlies strengthen across northern Australia as an anticyclone moves eastwards to the south of the continent. The synoptic situation is very similar to that for tropical cyclone Narelle (2013) described by Smith *et al.* 2015. There is a large expansion also in the area of the stronger monsoon westerlies ($> 10 \text{ m s}^{-1}$)

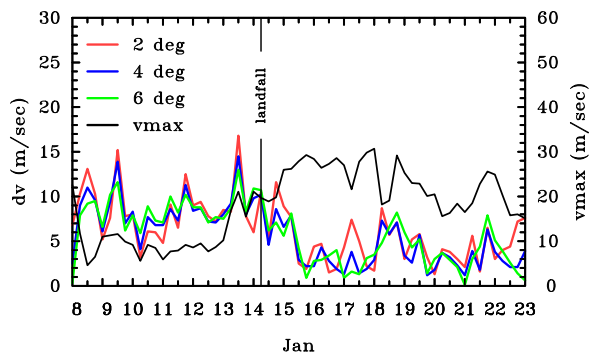


Figure 5. Mean vertical wind shear, characterized by the magnitude of the vector velocity difference between 850 mb and 200 mb, averaged over boxes $2^{\circ}\text{lon} \times 2^{\circ}\text{lat}$, $4^{\circ}\text{lon} \times 4^{\circ}\text{lat}$, and $6^{\circ}\text{lon} \times 6^{\circ}\text{lat}$ centred on the location of the minimum geopotential at 850 mb and maximum wind speed at 850 mb within the $2^{\circ}\text{lon} \times 2^{\circ}\text{lat}$ box.

between the equator and 10°S . Moreover, the circulation within the gyre increases and there is an accompanying lowering of the 850 mb geopotential heights near the centre of the gyre. It was at 01:30 UTC 13 Jan (shortly after the time shown in panel (e)) when a Tropical Cyclone Watch was issued for the possibility of the low developing into a tropical cyclone in 24–48 h. In Australia, bursts of monsoon activity are often associated with the Madden-Julian Oscillation (MJO), although the Australian Bureau of Meteorology announced on 7 Jan that the “MJO signal has been weak or indiscernible since late December. As the signal has been weak it is unlikely to have had a significant influence on tropical weather during this period. Forecasts of the MJO indicate that it is most likely to remain weak or indiscernible for at least another week.”

Figure 5 shows the magnitude of the mean vertical wind shear⁵ between 850 mb and 200 mb averaged over boxes $2^{\circ}\text{lat} \times 2^{\circ}\text{lon}$, $4^{\circ}\text{lat} \times 4^{\circ}\text{lon}$, and $6^{\circ}\text{lat} \times 6^{\circ}\text{lon}$ centred on the location of the minimum geopotential at 850 mb together with the maximum wind speed at 850 mb within the $2^{\circ}\text{lat} \times 2^{\circ}\text{lon}$ box. The latter serves as a measure of the system intensity. Until about 00 UTC 13 Jan, there was moderate vertical shear ($\approx 10 \text{ m s}^{-1}$) and the low did not intensify. Thereafter the vertical shear decreased in magnitude and the low intensified. The maximum wind speed nearly trebled in strength from about 10 m s^{-1} on 00 UTC 13 Jan to nearly 30 m s^{-1} on 16 Jan. Note that the average values of the shear over the three different sized boxes is very similar. From 06 14 Jan, the system was over land. It is not possible to conclude from the analyses that the decrease in vertical shear led to the intensification or whether the intensification, itself, led to the reduction in shear. Compared to tropical cyclone Narelle described in Smith *et al.* (2015), the low here suffered larger magnitudes of vertical shear during its genesis (the shear in the Narelle case was under 5 m s^{-1}) for most of the genesis period).

⁵The shear is characterized here by the magnitude of the vector velocity difference between the two levels, averaged over the box. We compute first the local vector velocity difference and then compute the average over the box. Because of the linearity of the shear vector calculation, the method is equivalent to computing the vector shear from the difference in the areal average velocity at the two levels. This is equivalent to the method adopted by DeMaria and Kaplan (1994, p213) as a basis for their Statistical Hurricane Intensity Prediction Scheme (SHIPS).

5.2. A vorticity perspective of formation and evolution

A vorticity perspective of the foregoing development is illustrated in the left panels of Fig. 6, which shows the vertical component of absolute vorticity together with the corresponding wind vectors and the contours of geopotential height at 850 mb. At 00 UTC on 9 Jan, the most prominent feature in the absolute vorticity is the broad region of elevated positive values⁶ over and south of Papua New Guinea. There is a weak circulation centred over the ocean south of Papua New Guinea at latitude 10°S , although the centre of the circulation has only sparse patches of enhanced vertical vorticity (values above 10^{-4} s^{-1}) at this time. The broad circulation encompasses also a region of low 850 mb geopotential heights. By 00 UTC on 11 Jan, the clump of absolute vorticity near the circulation has increased significantly in strength and areal extent, the recirculating winds show a commensurate increase in strength and the geopotential has lowered further. The vortex has moved to the west by this time, but has remained at latitude 10°S . By 00 UTC on 13 Jan, the circulation has strengthened and geopotential heights have dropped further. At this stage the system is relatively large in size with closed contours of geopotential heights about 10° longitude in diameter⁷. The size of this low is huge when compared to tropical cyclone Tracy (1974), which devastated Darwin on Christmas Day (Davidson 2010 and refs). The radius of gales in the case of Tracy was merely 50 km.

The right panels of Fig. 6 shows the distribution of the OW parameter at the 850 mb level from 00 UTC on 11 Jan to 00 UTC on 13 Jan. The major feature of the OW-field is the coherent region of positive values within the nascent vortex circulation centred near 10°S , while elsewhere in this flow positive OW-values are relatively small in scale. This major OW-feature is coherent up to 700 mb (not shown), and is one factor, at least, indicating that the vortex has the potential for further development. Although, as shown in Fig. 5, there was moderate vertical shear during these times, a factor that may have prohibited development. On 11 Jan the strongest patch of positive OW is located west of the vortex centre. During the next two days the areal extent of positive OW increases around this strong patch and the emergent vortex itself centres on this patch. The strength of the patch increases also during the three day time period.

As a step towards understanding the role of deep convection in the spin up of low-level vorticity, we examine next areas of strong upward velocity (vertical p-velocity $\omega < -0.5 \text{ Pa s}^{-1}$: a proxy for deep convection in the model) at 500 mb as the vortex evolves. These areas are shown in Fig. 7 with the horizontal wind fields at 850 mb superimposed. Figure 8 shows the corresponding fields of absolute vorticity at 850 mb with the advective flux vectors of absolute vorticity (\mathbf{F}_{af}) superimposed.

From 00 UTC 9 Jan until 00 UTC 11 Jan there are broadscale regions of disorganized vertical motion in the vicinity of the vortex centre. During this time the vectors \mathbf{F}_{af} indicate a flux of absolute vorticity around, and with a

⁶The sign of the vertical vorticity is reversed for similarity to Northern Hemisphere cases.

⁷Typically, forecasters describe storm size in terms of the outer core radius of gales (radius of the 17 m s^{-1} total winds) at a height of 10 m. In this case it is difficult to describe size in the conventional way as the system is embedded in a large region of background gale force winds near the surface, with the region of gales extending from 120° to 140°E (not shown).

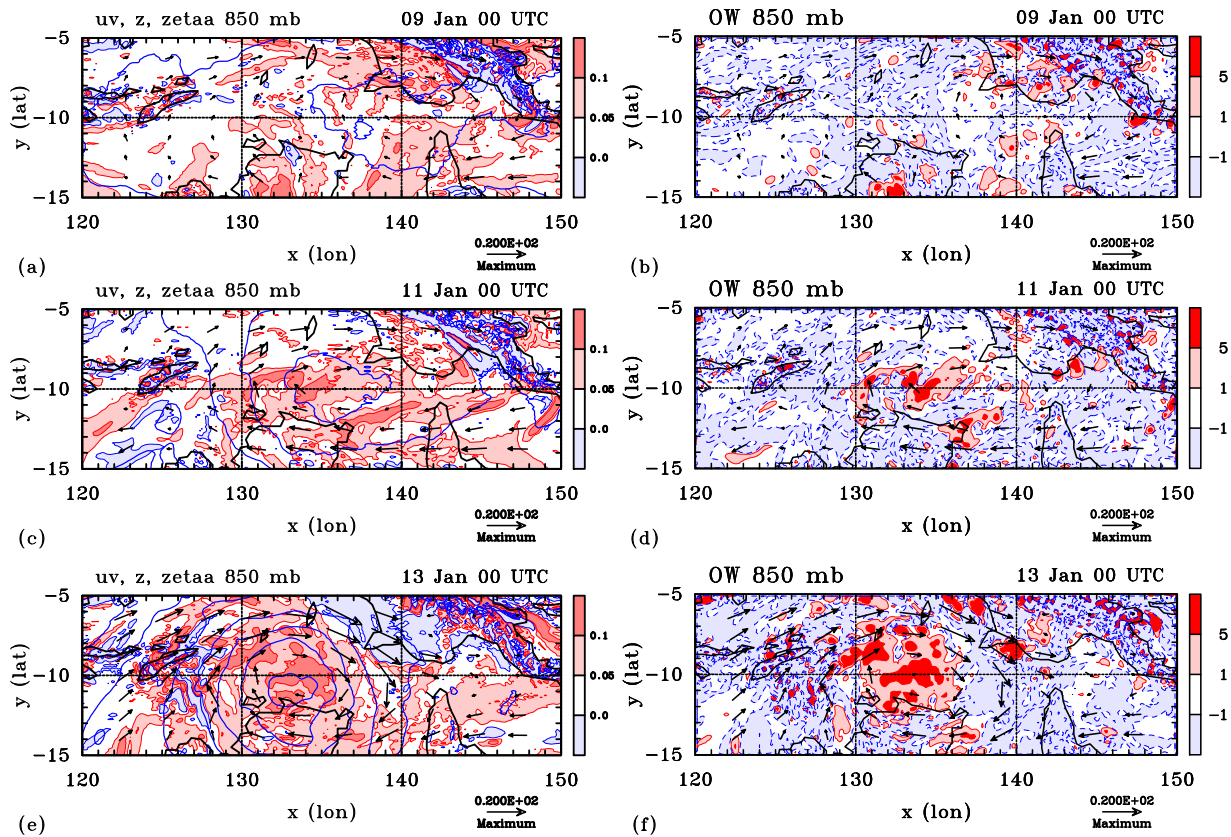


Figure 6. Left panels: Wind vectors at 850 mb together with contours of the absolute vorticity (shaded) and geopotential height (thick blue contours) at 00 UTC on (a) 9 Jan, (c) 11 Jan, and (e) 13 Jan 2014 illustrating the formation of the low. Contour interval for geopotential height 10 m. Absolute vorticity shading as shown on the label bar multiplied by 10^{-3} s^{-1} . Cyclonic values of vorticity are positive (red/pink shading), anticyclonic values are negative (light blue shading). Right panels: Contours of the Okubo-Weiss (OW) parameter (shaded) at 00 UTC on (b) 9 Jan, (d) 11 Jan, and (f) 13 Jan 2014 illustrating environment during the formation of the low. OW shading as shown on the label bar multiplied by 10^{-8} s^{-2} . Positive values have pink/red shading; negative values light blue shading. Wind vectors should be compared to the reference vector (20 m s^{-1}) at the bottom right of each panel.

component towards, the centre of circulation of the nascent vortex. In particular, on 9 and 10 Jan there is a large flux of absolute vorticity around from southern Papua New Guinea into the circulation centre.

By 12 Jan the regions of strong ascent have reorganized and now form an encircling band around the nascent vortex, with little convective activity in the inner core of the system. The cyclonic absolute vorticity has become consolidated around the developing vortex circulation. On 13 and 14 Jan, regions of strong vertical velocity occur closer to the circulation centre. It is during these two days that the maximum wind begins to increase notably within the $2^\circ \text{lon} \times 2^\circ \text{lat}$ box (see Fig. 5). Below the level of non-divergence, typically in the mid-troposphere, the upward motion leads to the low-level convergence of air, and therefore from the flux form of the vorticity equation to low-level convergence of absolute vorticity. In turn, this convergence leads to an amplification of the tangential wind field of the nascent vortex about the centre of circulation.

On the sub-vortex scale, there is a number of locally strong updraught cells in the model⁸, including one particularly intense cell near the centre of circulation as defined by the minimum of geopotential height at 850 mb. These cells must be contributing to the convergence of

absolute vorticity and material stretching of vortex tubes, equivalent to minus the divergence of the advective flux in the flux form of the vorticity equation, Eq. (1). Recalling the material form of the vorticity equation, it follows that as a vortex tube is stretched by an updraught, there will be a local amplification of both the vorticity and wind speed.

Figure 9 shows time-height cross sections of various quantities averaged over square boxes of $2^\circ \text{lon} \times 2^\circ \text{lat}$ and $10^\circ \text{lon} \times 10^\circ \text{lat}$ centred on the minimum geopotential at 850 mb. Highlighted also is the time at which landfall occurs. These quantities include the vertical mass flux (approximated here by $-\omega/g$), the temperature, the relative humidity, and the pseudo-equivalent potential temperature, θ_e . Shown also is a time-height cross section of the circulation around the box. Notable features of the vertical mass flux in the 2° box are the two “bursts” apparent at 18 UTC 13 Jan and 12 UTC 14 Jan. During the two day period from 00 UTC 13 Jan to 00 UTC 15 Jan, there is a notable increase in the maximum wind speed (from 8.7 m s^{-1} to 26.0 m s^{-1}) in the 2° box (shown in Fig. 5).

Early in the evolution of the low, up to 18 UTC 13 Jan, the main convective activity occurs outside the 2° box, but inside a 10° box. The circulation around the 2° box is weak until landfall occurs and the equivalent potential temperature averaged over the square box is generally low in the mid-troposphere before landfall. The convective burst just before landfall leads to a moistening of the mid- to upper-troposphere as seen in the relative

⁸Of course, the cells in the model do not represent individual observed updraughts. The ECMWF model uses a convective parameterization scheme.

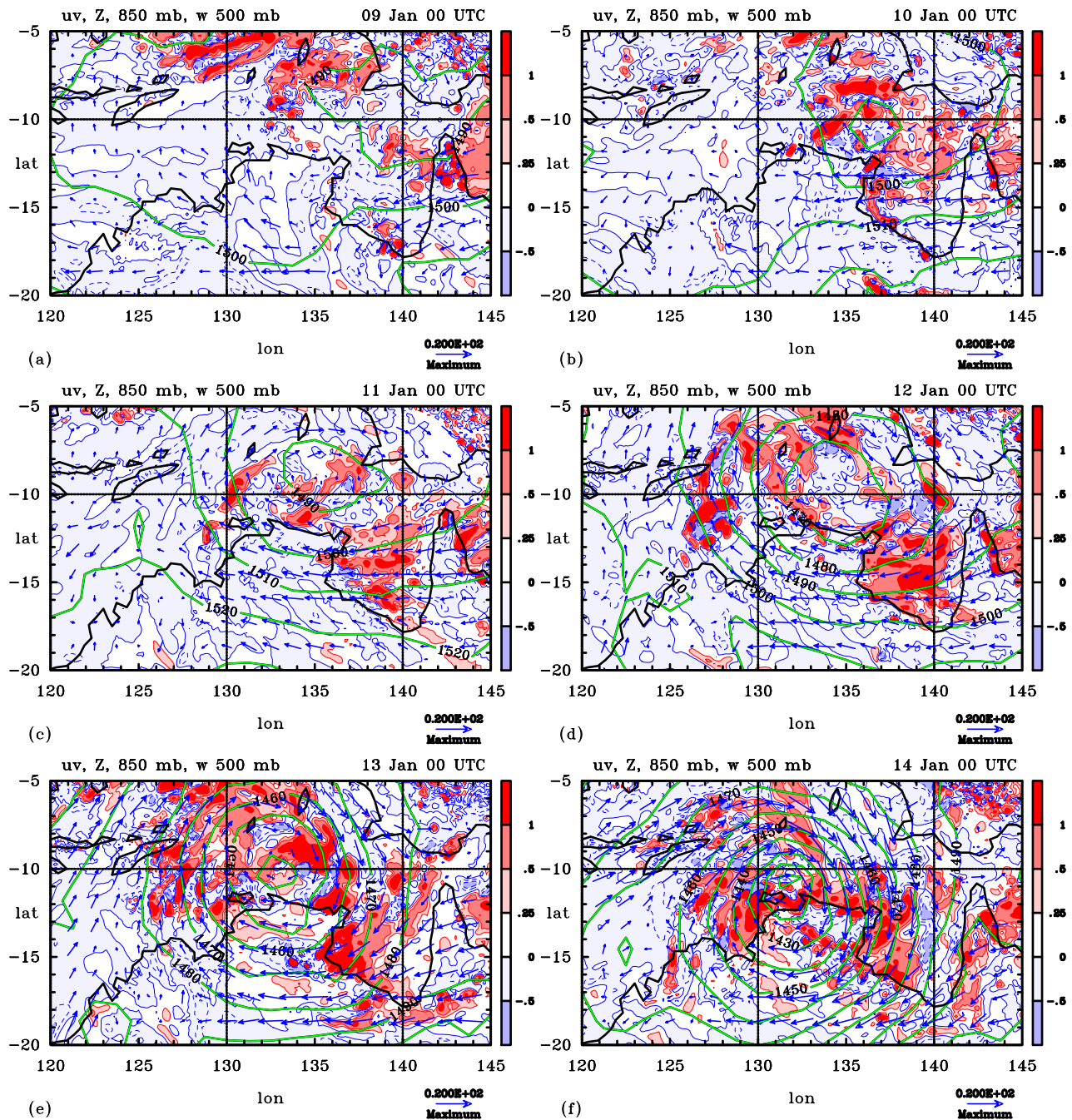


Figure 7. Wind vectors, contours of geopotential height together with contours of the vertical velocity at 500 mb at 00 UTC on several days in Jan 2014, illustrating the formation. Contour interval for geopotential height 10 m (green contours). Vertical p-velocity (ω) shading as shown on the label bar in units Pa s^{-1} . Upward vertical velocities (negative values of ω) are plotted as positive (red/pink shading); negative values of vertical velocity (positive values of ω) are plotted negative (light blue/blue shading). Wind vectors should be compared to the reference vector (20 m s^{-1}) at the bottom right of each panel.

humidity averaged over the square box. These convective bursts are accompanied by a temperature increase at upper levels. However, there are periods of slightly reduced temperature, mostly below 900 mb and mostly less than 0.5°C in magnitude. These are presumably associated with convectively-induced mesoscale downdraughts.

During the mature stage of the low and beyond, from 00 UTC 15 Jan to 00 UTC 21 Jan (Fig. 5), bursts of deep convective activity continue to occur in both the 2° and 10° boxes (Figures 9(a) and (b)). These bursts are interspersed with periods of mean subsidence, which tend to be accompanied by negative temperature anomalies at low

levels (pressures above 850 mb in Figure 9(c)). The mid-tropospheric minimum in θ_e continues to be progressively eroded through much of this period (Figure 9(e)) and the low-level circulation is maintained also (Figure 9(f)), despite the system being over land since 06 UTC 14 Jan.

In summary, the system formed in an environment with moderately high background vertical vorticity, but also with moderate vertical wind shear. It intensified following two days of sustained deep convective bursts that occurred close to the circulation centre. During this time, the vertical shear declined. The convective bursts generate low-level convergence of absolute vorticity, which leads to an amplification of the tangential wind field of the nascent

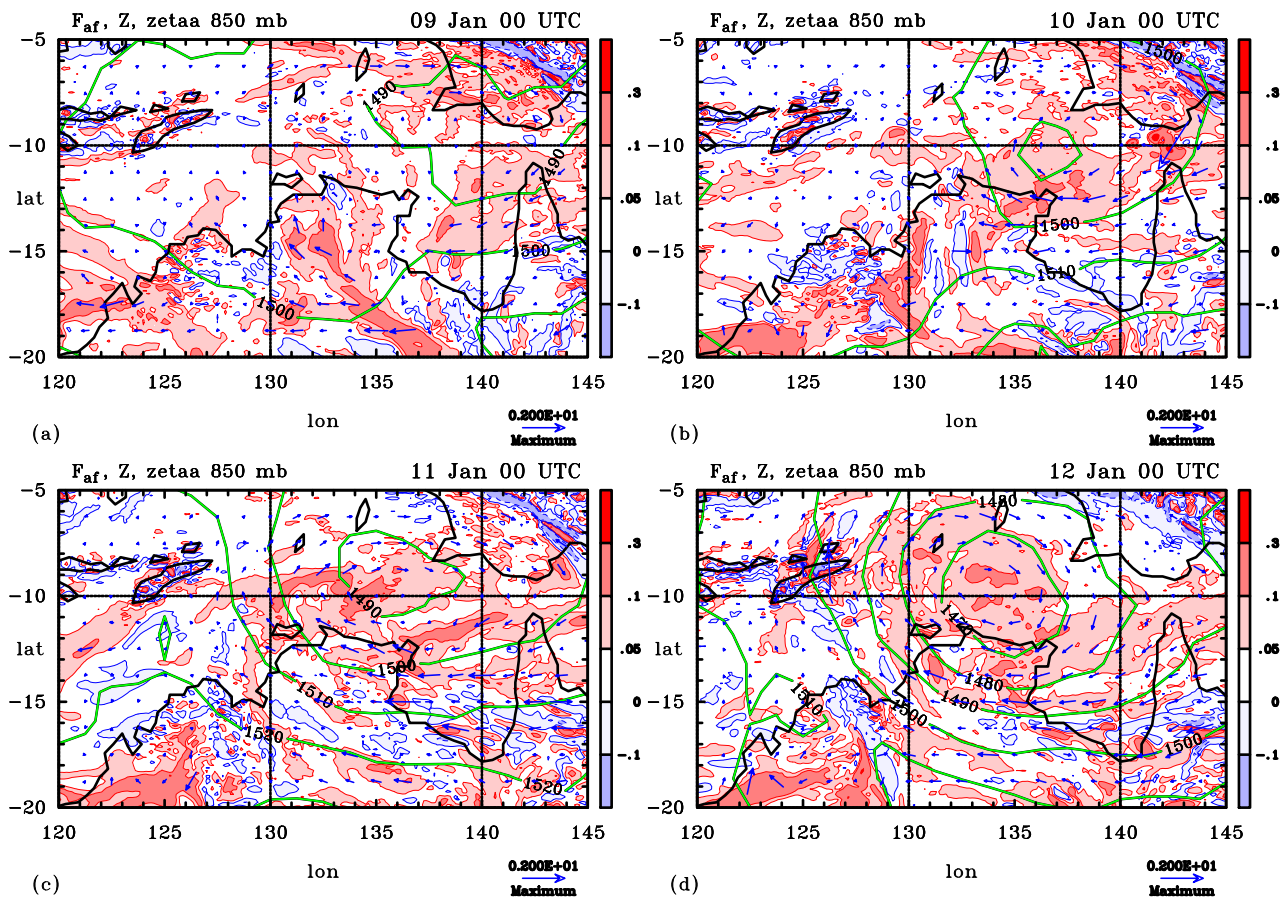


Figure 8. Vectors of the advective flux of absolute vorticity (F_{af}) with contours of geopotential height and shading of absolute vorticity at 850 mb at 00 UTC on several days in Jan 2014, illustrating the formation. Contour interval for geopotential height 10 m (green contours). Absolute vorticity shading as shown on the label bar multiplied by 10^{-3} s^{-1} . Cyclonic values of absolute vorticity are plotted as positive (red/pink shading); anticyclonic values of vorticity are plotted negative (light blue/blue shading). Vectors of the advective flux of absolute vorticity (multiplied by 10^{-3}) should be compared to the reference vector (2 m s^{-2}) at the bottom right of each panel.

vortex about the centre of circulation. The convective bursts moisten the mid- to upper-troposphere also, increasing both the relative humidity and equivalent potential temperature at these levels (shown in the next section). The aggregation of regions of enhanced cyclonic vorticity overlapping with coherent regions of positive values of OW within the nascent vortex circulation are important elements of the marsupial paradigm.

5.3. Moisture supply over land

The focus of this section is to gain insight into how the low was able to intensify and persist over land in the absence of strong moisture fluxes from the ocean. Emanuel *et al.* (2008) suggested that the intensification of warm-core cyclones over land in Northern Australia can occur when the underlying soil is sufficiently warm and wet and the system is maintained by latent heat transfer from the soil. They state that “when the storms are sufficiently isolated from their oceanic source of moisture, the rainfall they produce is insufficient to keep the soil wet enough to transfer significant quantities of heat, and the storms then decay rapidly”. The argument presented by Emanuel *et al.* (2008) is presumably influenced by the need for significant surface fluxes of moisture to give intensification in their model.

Recall from Fig. 5 that following landfall (at 06 UTC 14 Jan) the maximum wind speed increased following a

continued reduction of the vertical wind shear. Figure 9 shows that after landfall the relative humidity and equivalent potential temperature averaged over a 2° box were higher. There was a large burst of convective activity within the 2° box just after landfall and some smaller bursts at later times, the most notable being apparent at 12 UTC 15 Jan. The average vertical mass flux over a 10° box suggests that convection was still occurring in the low, but not always near to the circulation centre. After landfall the circulation increased in strength around the 2° box, increasing in depth to around 400 mb until 17 Jan.

We examine now the moisture budget for a mesoscale column of air. The budget may be written as:

$$\frac{\partial Q}{\partial t} = E - P + MC, \quad (2)$$

where $\partial Q/\partial t$ is the change in TPW with time, E is the rate of evaporation of moisture from the surface, P is rate of moisture loss by precipitation and MC is the rate of moisture convergence. Precipitation and evaporation are variables available in the ECMWF forecast data, while moisture convergence is calculated by vertically integrating the fluxes of moisture into a box centred on the system. These three quantities are then averaged over the area of the box to provide units of $\text{kg s}^{-1} \text{ m}^{-2}$.

Figure 11 shows sources and sinks of moisture obtained from Eq. 2 averaged over boxes $2^\circ\text{lon} \times 2^\circ\text{lat}$, $4^\circ\text{lon} \times 4^\circ\text{lat}$, and $6^\circ\text{lon} \times 6^\circ\text{lat}$ centred on the location of the minimum

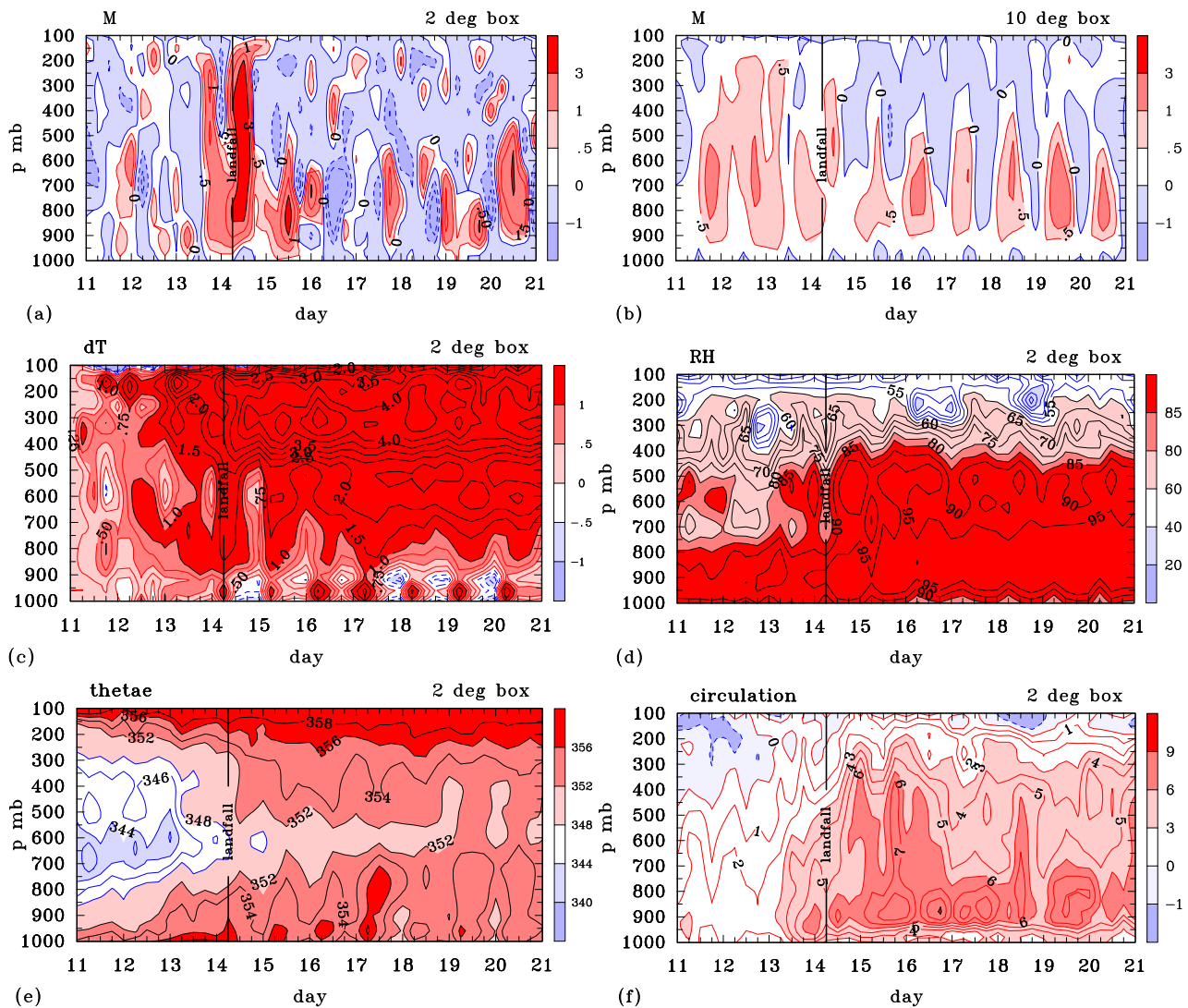


Figure 9. Time-height cross sections of system averaged quantities within a box $2^\circ\text{lon} \times 2^\circ\text{lat}$ and $10^\circ\text{lon} \times 10^\circ$, centred on the location of the minimum geopotential at 850 mb. These include (a,b) the vertical mass flux per unit area (units $\text{kg m}^{-2} \text{s}^{-1}$), (c) the temperature deviation from that at the start of the time series, (d) the relative humidity (in percent), and (e) pseudo-equivalent potential temperature (in K). Panel (f) shows the normalized circulation around the box (units m s^{-1}).

geopotential at 850 mb from 8 to 22 Jan. Shown also is the TPW averaged over the corresponding box. A key feature is that at most times the fluxes of moisture into the sides of the 2° box are equal to or larger than the amount of moisture lost by precipitation, the surface moisture fluxes make only a small contribution to the overall budget. A similar result has been found also for tropical cyclones (e.g. Kurihara 1975; Braun 2006; Trenberth et al. 2007).

By itself, the availability of substantial column moisture does not mean that deep convection will occur or be sustained. Deep convection requires the presence of conditional instability and sustained deep convection requires that this instability be maintained. Thus, while surface moisture fluxes are a small component of the overall moisture budget, they are important in maintaining conditional instability in the central region of the vortex. This maintenance is important in supporting deep convection there, which is necessary for the intensification process. Indeed, Malkus and Riehl (1960) pointed out that a prerequisite for hurricanes to be able to form was an elevation of θ_e in the central region by surface moisture flux

from the ocean⁹. Panel (e) of Figure 9 does show, *inter alia*, an increase in low-level θ_e averaged over the 2° box as the system develops, even while it is over land, suggesting that surface moisture fluxes are playing a role in the increase. As expected, after the low moves over land, the magnitude of the surface moisture flux decreases and a marked diurnal cycle becomes evident. This diurnal cycle is presumably a consequence of the daytime insolation over land.

A comparison of surface moisture fluxes over both land and sea is provided by Figure 10, which shows the patterns of the fluxes at 00 UTC on 14, 16, 18 and 20 Jan. On 14 Jan the moisture fluxes are largest over the sea north of Darwin, while fluxes over the continental Australia are small (typically less than 100 W m^{-2}). Two days later when the low is further inland there are somewhat enhanced moisture fluxes over land behind the low (there are regions with values between 300 and 400 W m^{-2}) where there had been copious amounts of precipitation on the previous days

⁹Based on hydrostatic considerations alone, Malkus and Riehl estimated that for typical conditions in a hurricane, a fall in surface pressure of 1 mb would require an elevation of θ_e by 0.4 K .

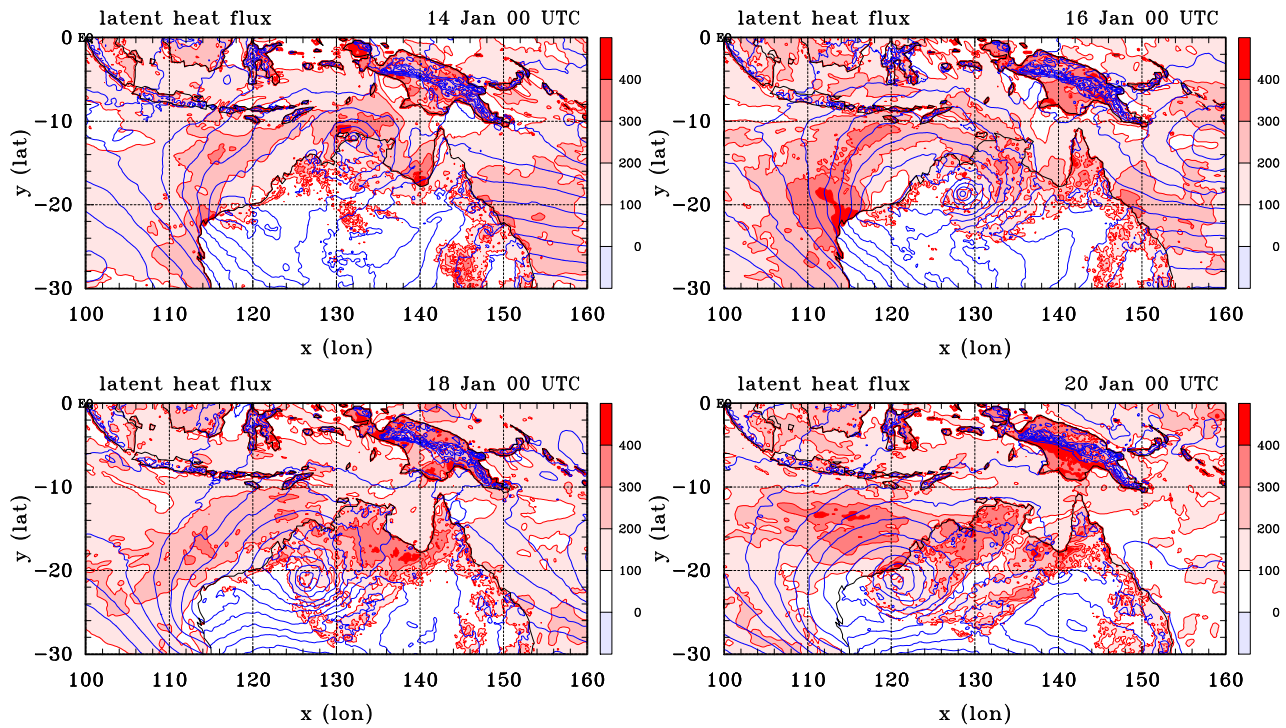


Figure 10. Exchange of latent heat with the surface through turbulent diffusion with contours of geopotential height for 14, 16, 18 and 20 Jan 2014 at 00 UTC. Shading as shown on the label bar in units W m^{-2} . Contour interval for geopotential height 10 m (blue contours).

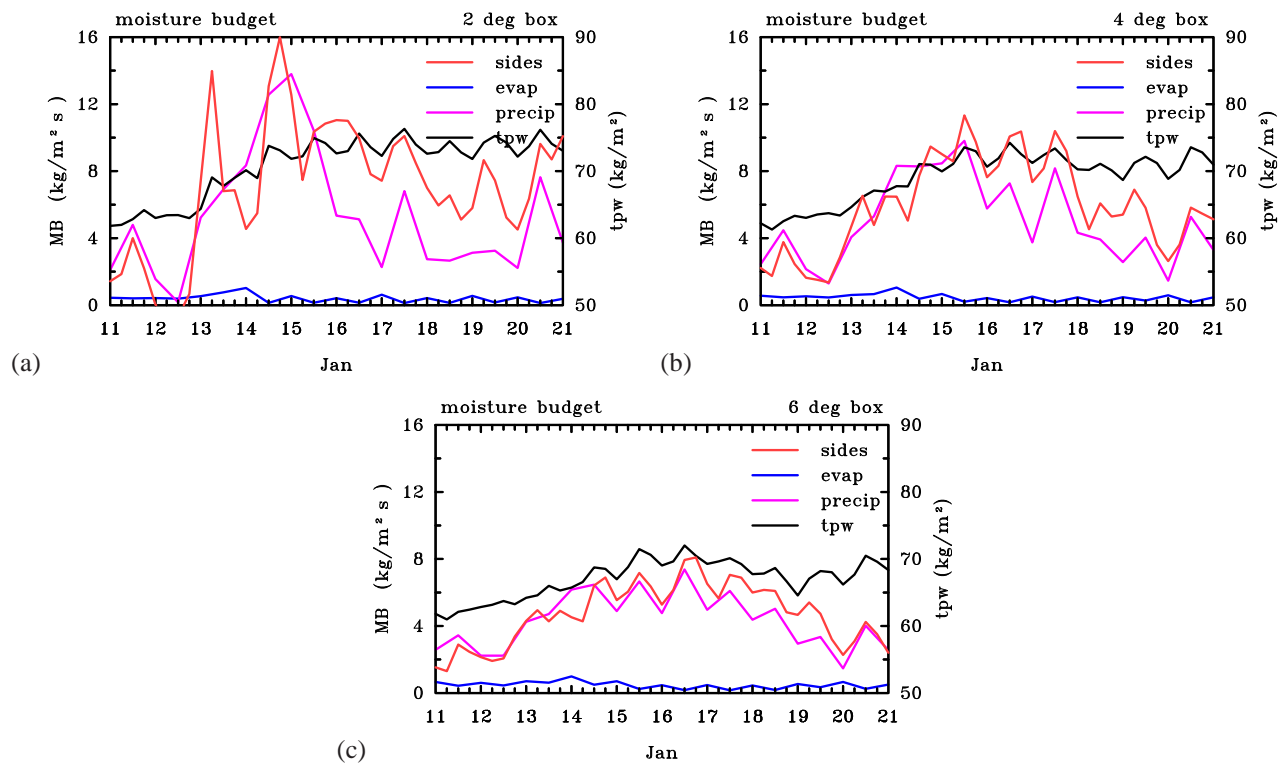


Figure 11. Sources and sinks of moisture including the contributions by surface evaporation, precipitation and the horizontal transport of moisture averaged over boxes (a) $2^\circ\text{lon} \times 2^\circ\text{lat}$, (b) $4^\circ\text{lon} \times 4^\circ\text{lat}$, and (c) $6^\circ\text{lon} \times 6^\circ\text{lat}$ centred on the location of the minimum geopotential at 850 mb. The horizontal transport of moisture is calculated by summing the vertically integrated fluxes of moisture into the box and then dividing the sum by the area of the box so that all terms have the units $\text{kg m}^{-2} \text{s}^{-1}$. The values shown here have been multiplied by 10^9 . Shown also is the total precipitable water in kg m^{-2} . A discussion of how the moisture budget is calculated and some issues about closure are found in section 5.3.

(see section 3). Over the next four days there are enhanced fluxes over land behind the low. It is notable that large values of surface moisture fluxes occur regularly over Papua

New Guinea indicating that significant moisture fluxes can occur over land if there is sufficient rainfall.

Returning to Figure 11, another feature worth noting is that the peak precipitation occurs between 14 and 16

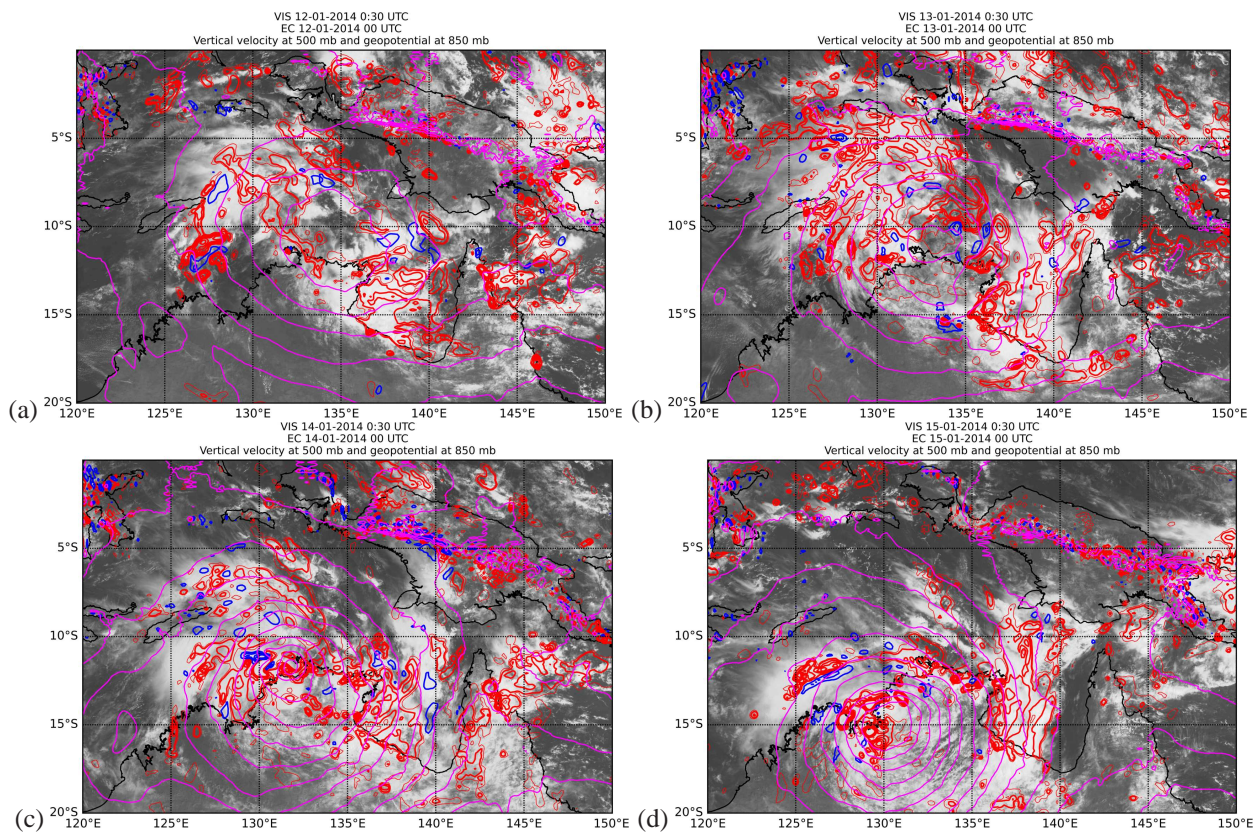


Figure 12. Visible satellite imagery from the MTSAT geostationary satellite half an hour after 00 UTC on (a) 12 Jan, (b) 13 Jan, (c) 14 Jan and (d) 15 Jan 2014 with contours of vertical motion (ω) at 500 mb from the ECMWF analyses at the 00 UTC times. Shown also are contours (pink) of geopotential heights. Contour interval: thin red contour $2.5 \times 10^{-1} \text{ Pa s}^{-1}$, thick contours begin at $5 \times 10^{-1} \text{ Pa s}^{-1}$ and increase in intervals of $5 \times 10^{-1} \text{ Pa s}^{-1}$. Red contours denote upward motion ($\omega < 0$), blue contours subsidence. Contour interval for geopotential heights 10 m.

Jan in the 2° box, corroborating the forecasters analysis in section 3. In all boxes, the TPW increases until about 16 Jan and then it remains approximately constant. Inspection of Figure 11 indicates that there is a period when the TPW remains approximately constant, even though the sum of terms on the right-hand-side of Eq. 2 is positive. Apparently, the moisture budget is not closed, especially in the 2° box. The reasons for this may lie partly in the fact that water substance is not strictly a conserved quantity in many models (e.g. Braun 2006), but also because the data available from the ECMWF system have certain deficiencies¹⁰.

Figure 12 shows the visible geostationary satellite imagery at 0030 UTC on 12, 13, 14 and 15 Jan, half an hour later than the ECMWF analysis fields. To ascertain the ability of the ECMWF analysis to capture the observed location of organized convective regions, the vertical motion from the analyses at 500 mb and the geopotential at 850 mb are superimposed on the satellite imagery. At 00 UTC on 12 Jan, the analysis shows several convective systems near the low but there is essentially no convection

in the vortex centre. Most of modeled regions of convective activity are overlapping or close to observed systems. The comparison at 00 UTC 13 Jan is similar, with the satellite observations confirming the lack of convective activity near the circulation centre. In particular, the banded cloud structures wrapping around the circulation centre in the visible imagery are captured qualitatively well by the model. However, the analysis has ascent north of the “Top End”, which is not observed. At 00 UTC on 14 and 15 Jan, the model produces strong convection within the inner core of the system, consistent with the observations. These two times (00 UTC on 14, 15 Jan) encompass the rapid intensification phase and there is generally a very good match between regions of deep convection captured by the analyses and that observed. The foregoing comparisons give confidence that the analyses have adequate skill in reproducing the broadscale convective features that are observed.

In summary, we have shown that the horizontal transport of moisture into a box (for all box sizes analyzed here) following the low is essentially equal to (or greater than) the moisture lost by precipitation. The contribution to the moisture budget by surface fluxes is small in comparison. Nevertheless, the small moisture fluxes play an important role in generating convective instability in a monsoon environment that already has relatively high values of TPW so that deep convective bursts can continue to occur even when the system is located far inland. The ECMWF analyses captured well the peak precipitation between 14

¹⁰There are many potential sources of error preventing closure in the moisture budget besides lack of conservation of total water. First, the precipitation and surface fluxes are not obtained from the analyses, but constructed from a time average of a 3 hour forecast from the valid time. These forecasts data are available only at 12 hourly intervals. The foregoing precipitation and surface flux data are compared with the instantaneous moisture convergence into the moving box computed from the 6 hourly analysis data. Estimation of the translation speed of the box from 6 hour analyses will introduce additional errors. Finally, TPW is calculated at 6 hourly intervals and calculation of its time tendency is subject to error also.

and 16 Jan, corroborating the forecaster's analysis in section 3.

6. Conclusions

We have presented an analysis of a tropical low that formed in the Australian monsoon in January 2014 and its subsequent intensification over land based on European Centre for Medium Range Weather Forecasts analyses. Interpretations of the formation were given in terms of vorticity dynamics and related elements of the marsupial paradigm of tropical cyclogenesis. Support for the intensification was examined also from a moisture budget. The analyses indicated that the intensification of the low required repeated bursts of deep convection near the centre of the gyre to promote the further concentration of same-sign vorticity near the centre. This concentration of vorticity increased the local circulation about the centre, which amounts to increasing the local tangential wind speed and, through approximate gradient wind balance above the boundary layer, to a lowering of the central pressure.

The low began to develop over water in moderate deep-layer shear, but in an environment with moderately high background vertical vorticity following two days of sustained convective bursts close to the circulation centre. These convective bursts moistened the mid- to upper-troposphere, increasing both the relative humidity and equivalent potential temperature at these levels as depicted by a mesoscale (2°) box following the system. After the system made landfall, the horizontal transport of moisture into this box following the low is essentially equal to (or greater than) the moisture lost by precipitation, whereas surface moisture fluxes make only a small contribution to the overall budget. Nevertheless, enhanced surface moisture fluxes near the circulation centre play an important role in supporting deep convection and thereby the intensification process. The ECMWF analyses captured well the peak precipitation between 14 and 16 Jan, corroborating the forecaster's analysis.

The findings indicate that the processes of intensification are the same over land as those that operate over the ocean. All that is required is for deep convection to persist near the circulation centre, which requires an adequate import of moisture from the storm environment and a modest elevation of conditional instability near the storm centre to sustain deep convection there. There appears to be no need to invoke complex soil processes to explain intensification over land.

7. Acknowledgements

This work was motivated by a visit of the first three authors to the Australian Bureau of Meteorology's Regional Forecast Centre in Darwin during the monsoon season and the opportunity this visit provided to witness the monsoon first hand as well as the forecasting challenges it poses. We thank Todd Smith for his warm hospitality and support for our research. We thank also the many forecasters at the Regional Office who have shared their expertise with us. We thank also Denis Margetic from the Bureau of Meteorology Head Office for supplying us with satellite data and for code to plot these data. We are grateful to two anonymous reviewers, whose perceptive and constructive comments helped to improve the manuscript. GK and RKS acknowledges funding for

tropical cyclone research from the German Research Council (Deutsche Forschungsgemeinschaft) under Grant no SM30/23-4 and the Office of Naval Research Global under Grant No. N62909-15-1-N021. MTM acknowledges the support of NSF grant AGS-1313948, NOAA HFIP grant N0017315WR00048, NASA grant NNG11PK021 and the U.S. Naval Postgraduate School.

References

- Braun SA. 2006: High-resolution simulation of Hurricane Bonnie (1968). Part II: Water budget. *J. Atmos. Sci.*, **63**, 4364.
- Davidson NE, 2010: On the intensification and recurvature of tropical cyclone Tracy (1974). *Aust. Met. Ocean. Soc. Journl.*, **60**, 169-177.
- DeMaria M, Kaplan J. 1994: A Statistical Hurricane Intensity Prediction Scheme (SHIPS) for the Atlantic basin. *Wea. Forecasting*, **9**, 209-220.
- Dunkerton TJ, Montgomery MT, Wang Z. 2009: Tropical cyclogenesis in a tropical wave critical layer: easterly waves. *Atmos. Chem. Phys.*, **9**, 5587-5646.
- Emanuel K, 1995: The behavior of a simple hurricane model using a convective scheme based on subcloud-layer entropy equilibrium. *J. Atmos. Sci.*, **52**, 3959-3968.
- Emanuel K, DesAutels C, Holloway C, and Korty C, 2004: Environmental control of tropical cyclone intensity. *J. Atmos. Sci.*, **61**, 843-858.
- Emanuel K, Callaghan J, and Otto P, 2008: A hypothesis for the redevelopment of warm-core cyclones over Northern Australia. *Mon. Wea. Rev.*, **136**, 3863-3872.
- Evans C, Schumacher RS, Galarnreau TJ Jr. 2011: Sensitivity in the overland reintensification of tropical cyclone Erin (2007) to near-surface soil moisture characteristics. *Mon. Wea. Rev.*, **139**, 3848-3870.
- Haynes P, McIntyre ME, 1987: On the evolution of vorticity and potential vorticity in the presence of diabatic heating and frictional or other forces. *J. Atmos. Sci.*, **44**, 828-841.
- Kaplan J, and DeMaria, M. 1995: A simple empirical model for predicting the decay of tropical cyclone winds after landfall. *J. Appl. Meteor.*, **34**, 2499-2512.
- Kilroy G, Smith RK, 2013: A numerical study of rotating convection during tropical cyclogenesis. *Q. J. R. Meteor. Soc.*, **139**, 1255-1269.
- Kurihara Y. 1975: Budget analysis of a tropical cyclone simulated in an axisymmetric numerical model. *J. Atmos. Sci.*, **32**, 2559.
- Malkus JS, and Riehl H, 1960: On the Dynamics and Energy Transformations in Steady-State Hurricanes. *Tellus*, **12**: 1-20.
- McBride JL, Keenan TD. 1982: Climatology of tropical cyclone genesis in the Australian region. *J. Clim.*, **2**, 13-33.
- Molinari J, Lombardo K, and Vollaro D, 2007: Tropical cyclogenesis within an equatorial Rossby wave packet. *J. Atmos. Sci.*, **64**, 1301-1317.
- Montgomery MT, Nguyen SV, Smith RK and Persing J, 2009: Is WISHE essential for tropical cyclone intensification? *Q. J. R. Meteor. Soc.*, **135**, 1697-1714.
- Montgomery MT, Davis C, Dunkerton T, Wang Z, Velden C, Torn R, Majumdar SJ, Zhang F, Smith RK, Bosart L, Bell MM, Haase JS, Heymsfield A, Jensen J, Campos T, and Boothe MA, 2012: The Pre-Depression Investigation of Cloud Systems in the Tropics (PREDICT) Experiment:

Scientific basis, new analysis tools and some first results. *Bull. Amer. Met. Soc.*, **93**, 153-172.

Montgomery MT and Smith RK. 2014: Paradigms for tropical cyclone intensification. *Aust. Met. Ocean. Soc. J. Atmos. Sci.*, **64**, 37-66.

Montgomery MT, Persing J, and Smith RK, 2014: Putting to rest WISHE-ful misconceptions for tropical cyclone intensification. *J. Adv. Model. Earth Syst.*, **7**, 92-109.

Raymond, DJ, C. López Carillo, 2011: The vorticity budget of developing typhoon Nuri (2008). *Atmos. Chem. Phys.*, **11**, 147-163.

Raymond DJ, Gjorgjievska S, Sessions SL, Fuchs Z. 2014: Tropical cyclogenesis and mid-level vorticity. *Aust. Met. Ocean. Soc. J. Atmos. Sci.*, **64**, 11-25.

Rozoff CM, Schubert WH, McNoldy BD, and Kossin JP, 2006: Rapid filamentation zones in intense tropical cyclones. *J. Atmos. Sci.*, **63**, 325-340.

Sharkov EA, Shramkov YN, Pokrovskaya IV, 2012: Increased water-vapor content in the atmosphere of tropical latitudes as a necessary condition for the genesis of tropical cyclones. *Izvestiya, Atmospheric and Oceanic Physics*, **48**, 900-908.

Shen W, Ginis I, Tuleya RE, 2002: A numerical investigation of land surface water on landfalling hurricanes. *J. Atmos. Sci.*, **59**, 789-802.

Smith RK, Montgomery MT. 2015: Towards clarity on understanding tropical cyclone intensification. *J. Atmos. Sci.*, **72**, 3020-3031.

Smith RK, Montgomery MT, Kilroy G, Tang S, Müller SK. 2015: Tropical low formation during the Australian monsoon: the events of January 2013. *Aust. Met. Ocean. Soc. J. Atmos. Sci.*, in press.

Trenberth KE, Davis CA, Fasullo J. 2007: Water and energy budgets of hurricanes: Case studies of Ivan and Katrina. *J. Geophys. Res.*, **112**, doi:10.1029/2006JD008303, d23106.

Tory KJ, Kepert JD, Sippel JA, Nguyen CM. 2012: On the use of potential vorticity tendency equations for diagnosing atmospheric dynamics in numerical models. *J. Atmos. Sci.*, **69**, 942-960.